

# Discontinuities in driven spin-boson systems due to coherent destruction of tunneling: breakdown of the Floquet-Gibbs distribution

Georg Engelhardt<sup>1</sup>, Gloria Platero<sup>2</sup>, and Jianshu Cao<sup>1,3\*</sup>

<sup>1</sup>*Beijing Computational Science Research Center, Beijing 100193, Peoples Republic of China*

<sup>2</sup>*Instituto de Ciencia de Materiales de Madrid, CSIC, 28049 Madrid, Spain*

<sup>3</sup>*Department of Chemistry, Massachusetts Institute of Technology, 77 Massachusetts Avenue, Cambridge, Massachusetts 02139, USA*

(Dated: October 31, 2021)

We show that the probability distribution of the stationary state of a dissipative ac-driven two-level system exhibits discontinuities, i.e. jumps, for parameters at which coherent destruction of tunneling takes place. These discontinuities can be observed as jumps in the emission of the Mollow triplet. The jumps are the consequence of discontinuities in the transition rates, which we calculate numerically and analytically based on the secular Floquet-Redfield formalism.

**Introduction.** Due to the high experimental control, periodic driving has become a flexible tool for quantum state manipulation with various applications, e.g., for topological matter, quantum phase transitions, quantum transport, and even-harmonic generation [1–14]. As a quantum system is never completely decoupled from its environment, thermalization finally leads to a relaxation towards a stationary state. Yet, very little is known about possible stationary states of periodically-driven systems. In this letter, we report on exotic stationary states exhibiting probability jumps, which are related to two prominent effects, namely coherent destruction of tunneling (CDT) [15] and the Mollow triplet [16].

In a recent article, Shirai et al. have discussed under which special conditions effective Floquet-Gibbs states arise [17, 18]. The probabilities of these periodic Floquet states, characteristic states of periodically-driven systems, are determined by their corresponding *quasienergies*  $\epsilon_\lambda$  in a Gibbs-like fashion, thus  $p_\lambda \propto e^{-\beta\epsilon_\lambda}$ . However, given the richness of quantum effects in periodically-driven systems and their experimental control, the resulting stationary states are not necessarily Gibbs-Floquet states and can possibly exhibit intriguing features.

In isolated ac-driven systems, CDT is defined by an exact degeneracy of two quasienergies. Consequently, the dynamics in these levels is frozen as the effective Hamiltonian is zero [19–21]. The emission of an ac-driven two-level system ( $|0\rangle, |1\rangle$ ) coupled to an environment (sketched in Fig. 1(a)) can exhibit a Mollow triplet as sketched in Fig. 1(b) [16, 22, 23]. Thereby, the driving field with frequency  $\Omega$  induces transitions between the states which are accompanied by emitting a photon (or phonon, which we focus here) with frequencies  $\Omega - \Delta$  ( $|0\rangle \rightarrow |1\rangle$ ),  $\Omega$  ( $|0\rangle \rightarrow |0\rangle$  and  $|1\rangle \rightarrow |1\rangle$ ), and  $\Omega + \Delta$  ( $|1\rangle \rightarrow |0\rangle$ ). Here,  $\Delta$  denotes the difference between two quasienergies. The emitted phonons can be blue shifted  $I_{b(\text{lue})}$ , unshifted or red shifted  $I_{r(\text{ed})}$ , respectively. Clearly, the unshifted transitions do not change the

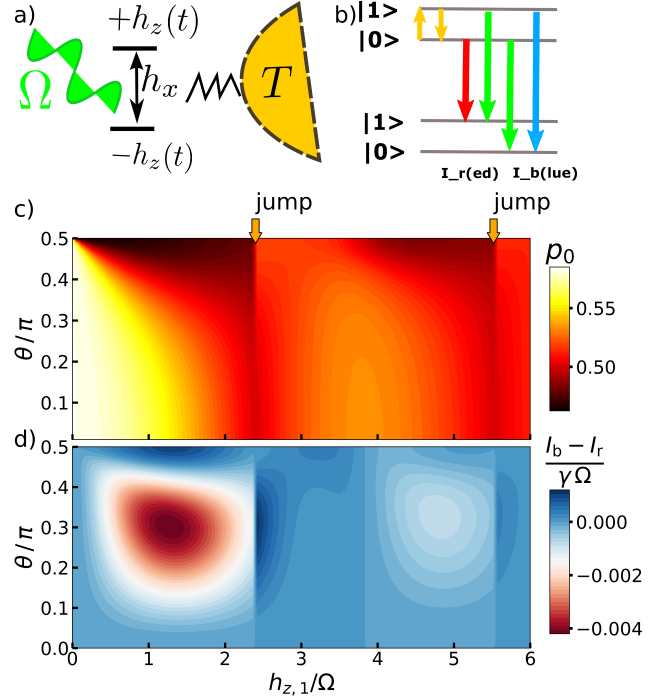


FIG. 1. (a) The spin-boson model is driven with frequency  $\Omega$ . Due to the internal coherent dynamics, it emits phonons with  $\Omega, \Omega \pm \Delta$  (unshifted, blue shifted, red shifted). The corresponding transitions are depicted in (b). (c) shows the probability of the Floquet state for  $\lambda = 0$  as a function of the coupling angle  $\theta$  and the driving amplitude  $h_{z,1}$ . (d) depicts the difference of the emitted blue and red shifted phonons into the bath. The offset energy splitting  $h_{-rmz,0} = 0$ , cut-off frequency  $\omega_c = 10h_x$ , driving frequency  $\Omega = 40h_x$  and temperature  $k_B T = 3h_x$  are expressed in units of the tunneling amplitude  $h_x$ .

system state, but the shifted transitions can be used to control it.

Our main findings are summarized in Fig. 1 (c) and (d), where we depict the probability of the Floquet state with the lowest quasienergy  $p_0$  and the difference of emitted phonons  $I_b - I_r$  as a function of driving amplitude  $h_{z,1}$

\* jianshu@mit.edu

and a system-environment coupling angle  $\theta$ . Remarkably, we observe jumps in both observables at specific values of the driving amplitude, marked with arrows in Fig. 1 (c) and (d). As we will explain in detail, they appear at parameters, at which CDT takes place.

**Model system.** We consider a generic two-level system, which describes, e.g., the low-energy physics of a double-well potential or a superconducting qubit. It is externally driven and coupled to a thermal environment as sketched in Fig. 1(a). The Hamiltonian reads

$$H(t) = \frac{h_x}{2} \sigma_x + \frac{h_z(t)}{2} \sigma_z + \hat{\sigma}_\theta \sum_k V_k (b_k + b_k^\dagger) + H_B, \quad (1)$$

where  $\sigma_\alpha$  with  $\alpha = \{x, y, z\}$  denote the Pauli matrices,  $h_x$  denotes the tunneling amplitude and  $h_z(t) = h_{z,0} + h_{z,1} \cos(\Omega t)$  is the time-dependent energy splitting, where  $h_{z,0}$  is the offset,  $h_{z,1}$  is the driving amplitude and  $\Omega$  is the driving frequency. The bath is quadratic in bosonic operators  $b_k$  and is coupled via the system operator  $\hat{\sigma}_\theta = \sin \theta \sigma_x + \cos \theta \sigma_z$  with strengths  $V_k$ . Depending on the coupling angle  $\theta$ , it is known that undriven systems can give rise to diverse physical behavior [24–28].

Floquet theory describes the dynamics of periodically-driven systems [29, 30]. Due to the periodic system dynamics with frequency  $\Omega = 2\pi/\tau$ , there are characteristic states of the system which fulfill  $|\Phi_{n,\lambda}(t)\rangle = e^{-i\epsilon_{n,\lambda}t} |\varphi_{n,\lambda}(t)\rangle$ , with quasienergy  $\epsilon_{n,\lambda}$  and periodic Floquet state  $|\varphi_{n,\lambda}(t)\rangle = |\varphi_{n,\lambda}(t + \tau)\rangle$ . These states are the analogue to the eigenstates in time-independent systems. Importantly, the Floquet states  $\lambda$  are not uniquely defined due to the Brillouin zone index  $n$ : a state with index  $n$  can be related to the  $n = 0$  state by  $\epsilon_{n,\lambda} = \epsilon_{0,\lambda} + n\Omega$  and  $|\varphi_{n,\lambda}(t)\rangle = e^{-in\Omega t} |\varphi_{0,\lambda}(t)\rangle$ . The stroboscopic Floquet states are the eigenstates of the time-evolution operator after one period  $\hat{U}_s(\tau) |\varphi_{n,\lambda}(0)\rangle = e^{-i\epsilon_{n,\lambda}\tau} |\varphi_{n,\lambda}(0)\rangle$ .

In Fig. 2(a), we depict the numerically calculated quasienergies  $\epsilon_\lambda = \epsilon_{0,\lambda}$  as function of  $h_{z,1}/\Omega$ . Here, the index  $\lambda$  can take the values  $\lambda = 0, 1$  and we consider  $n = 0$ . The stroboscopic dynamics follows the effective Hamiltonian  $H_{\text{eff}} = \frac{h_{z,0}}{2} \sigma_z + \frac{h_x}{2} \mathcal{J}_0(h_{z,1}/\Omega) \sigma_x + \mathcal{O}(\frac{1}{\Omega})$ . For  $h_{z,0} = 0$ , we find  $\epsilon_\lambda = \pm \frac{h_x}{2} \mathcal{J}_0(h_{z,1}/\Omega)/2$ , so that there are degeneracies at the roots of the Bessel function  $\mathcal{J}_0(h_{z,1}/\Omega) = 0$ . This is the celebrated CDT effect, as the dynamics at these parameters is frozen. The stroboscopic Floquet states read  $|\varphi_\lambda(0)\rangle \approx |\text{sign}[\mathcal{J}_0(h_{z,1}/\Omega)] (-1)^\lambda\rangle_x$ . Accordingly, there is a non analytic crossover of the Floquet state, e.g.  $|\varphi_0(0)\rangle = |-1\rangle_x$  to  $|\varphi_0(0)\rangle = |+1\rangle_x$ , at the roots of the Bessel function. As we explain, the crossover of the Floquet states is the origin of the probability jumps observed in Fig. 1.

**Rate equations.** An important point to realize is that though the states  $|\varphi_{n,\lambda}(t)\rangle$  of the spin system are equivalent for different  $n$  in a closed system,  $n$  becomes physically relevant when the system is coupled to a thermal bath  $H_B$ . In this situation, the bath can trigger transitions between different Brillouin zones  $n, n'$ . In Fig. 1(b) we illustrate transitions associated with

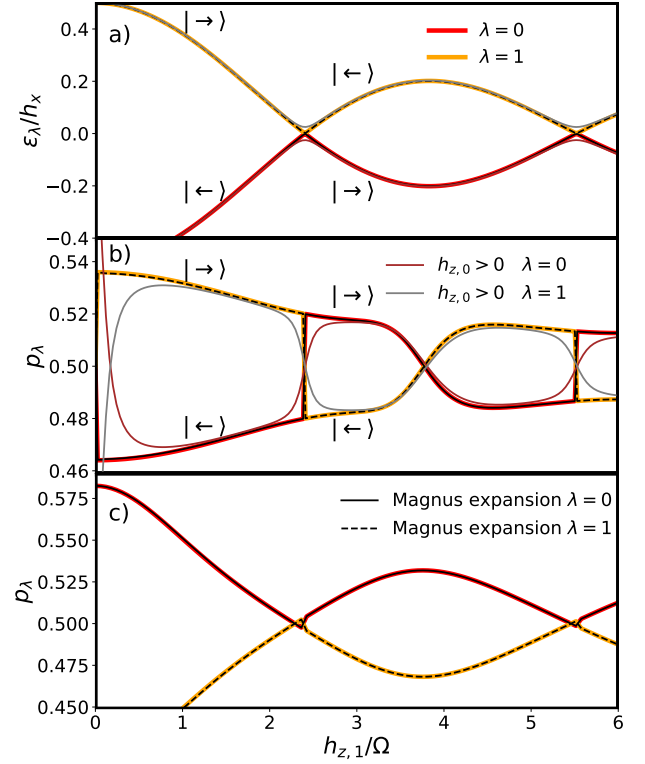


FIG. 2. (a) The quasienergy spectrum as a function of the driving amplitude  $h_{z,1}$ . (b) and (c) depict slices of Fig. 1(c) showing both stationary Floquet state probabilities  $p_\lambda$  for  $\theta = \pi/2$  ( $\hat{\sigma}_{\pi/2} = \sigma_x$ ) and  $\theta = \pi/4$  ( $\hat{\sigma}_{\pi/4} = \frac{1}{\sqrt{2}}\sigma_x + \frac{1}{\sqrt{2}}\sigma_z$ ), respectively. The Floquet states are approximately given by the eigenstates of  $\sigma_x$ , which we denote by  $|-1\rangle_x, |+1\rangle_x$  corresponding to eigenvalues  $-1, 1$ , respectively.

$\Delta n = n - n' = -1$ . Using the secular Floquet-Redfield formalism [30, 31], one can derive the rate equations

$$\begin{aligned} \frac{d}{dt} p_0 &= - \sum_{\Delta n} A_{1 \leftarrow 0}^{(\Delta n)} p_0 + \sum_{\Delta n} A_{0 \leftarrow 1}^{\Delta n} p_1, \\ \frac{d}{dt} p_1 &= + \sum_{(\Delta n)} A_{1 \leftarrow 0}^{(\Delta n)} p_0 - \sum_{\Delta n} A_{0 \leftarrow 1}^{(\Delta n)} p_1, \end{aligned} \quad (2)$$

where  $p_\lambda$  denotes the probability to be in Floquet state  $\lambda$  and  $A_{\lambda \leftarrow \mu}^{(n)}$  is the transition probability between Floquet states

$$\begin{aligned} A_{\lambda \leftarrow \mu}^{(n)} &= \Gamma(\Delta_{\lambda\mu}^n) [n_B(\Delta_{\lambda\mu}^n) + 1] \cdot |a_{\lambda \leftarrow \mu}^n|^2, \\ a_{\lambda \leftarrow \mu}^{(n)} &= \frac{1}{\tau} \int_0^\tau \langle \varphi_\lambda(0) | \hat{\sigma}_\theta(t) | \varphi_\mu(0) \rangle e^{-in\Omega t} dt. \end{aligned} \quad (3)$$

Here,  $n_B(\omega)$  denotes the Bose distribution and  $\Gamma(\omega) = \sum_k V_k^2 \delta(\omega - \omega_k) = \gamma\omega/(\omega^2 + \omega_c^2)$  (coupling strength  $\gamma$ , cut-off frequency  $\omega_c$ ) denotes the coupling density, which we define for negative frequencies by  $\Gamma(\omega) = -\Gamma(-\omega)$ , and  $\Delta_{\lambda\mu}^n = \epsilon_\mu - \epsilon_\lambda - n\Omega$ . The time-dependent operator

reads  $\hat{\sigma}_\theta(t) = e^{i\hat{\Lambda}(t)} \hat{\sigma}_\theta e^{-i\hat{\Lambda}(t)}$ , where  $\hat{\Lambda}(t)$  is defined by

$$|\varphi_\lambda(t)\rangle = e^{-i\hat{\Lambda}(t)} |\varphi_\lambda(0)\rangle, \quad (4)$$

at which the operator  $e^{-i\hat{\Lambda}(t)}$  propagates the Floquet states.

It is easy to show that the coefficients fulfill  $a_{\lambda\leftarrow\mu}^{(n)} = (a_{\mu\leftarrow\lambda}^{(-n)})^*$ . As a consequence, the related rates obey the detailed balance condition  $A_{\lambda\leftarrow\mu}^{(n)} = A_{\mu\leftarrow\lambda}^{(-n)} e^{\Delta_{\lambda\mu}^{(n)}/T}$ , where  $T$  is the temperature of the environment. Yet, in general  $|a_{\mu\leftarrow\lambda}^{(n)}| \neq |a_{\lambda\leftarrow\mu}^{(n)}|$ , which gives rise to a break down of the detailed balance relation in the stationary state, thus  $p_0/p_1 \neq e^{-\Delta/T}$  with  $\Delta = \epsilon_1 - \epsilon_0$ .

**Stationary state.** Figures 2(b) and (c) depict the stationary state probabilities for the coupling  $\hat{\sigma}_\theta$  with  $\theta = \pi/2, \pi/4$ , respectively. For  $\theta = 0, \pi$ , the system approaches a Floquet-Gibbs state according to Ref. [18]. In (b), we find a probability inversion for small  $h_{z,1}/\Omega$  and probability jumps at the roots of the Bessel function  $\mathcal{J}_0(h_{z,1}/\Omega) = 0$ . These effects can be explained by analyzing the rates in Eq. (3). Due to a generalized parity symmetry,  $A_{\lambda\leftarrow\mu}^{(0)}$  vanishes exactly [32]. Consequently, the rate equations are dominated by the transitions  $\Delta n = -1$ , as  $n_B(|\Delta_{\lambda\mu}^{n>0}|) \ll 1$  for  $\Delta n > 0$  due to a large energy difference  $\Delta_{\lambda,\mu}^{n,\mu} \approx -n\Omega$ , i.e., the transitions marked by the red and blue arrows in Fig. 1(b) (green transitions do not change the state). The corresponding coefficients  $|a_{\mu\leftarrow\lambda}^{(-1)}|^2$  are depicted in Fig. 3(a), where we observe that  $|a_{1\leftarrow 0}^{(-1)}|^2 > |a_{0\leftarrow 1}^{(-1)}|^2$  for, e.g.,  $h_{z,1}/\Omega < z_0$ , with  $z_0$  denoting the first root of the zeroth-order Bessel function. As  $n_B(\Delta_{\lambda\mu}^n) \ll 1$  and  $\Gamma(\Delta_{10}^{(-1)}) \approx \Gamma(\Delta_{01}^{(-1)})$ , we find from Eq. (2) that  $p_1/p_0 \approx |a_{1\leftarrow 0}^{(-1)}|^2 / |a_{0\leftarrow 1}^{(-1)}|^2$  which explains the probability inversion. The rates explain the jump in the probability distribution. In Fig. 3(a) we observe jumps at the CDT positions. The jump is magnified in Fig. 3(b). The non-continuous behavior becomes more clear when considering Eq. (3). At the CDT, the Floquet states switch, thus  $|\varphi_\lambda(0)\rangle \leftrightarrow |\varphi_\mu(0)\rangle$ , which gives rise to the non-analytic behavior.

A similar reasoning can be applied to the  $\hat{\sigma}_{\pi/4}$  coupling depicted in Fig. 2(c). Away from the CDT, the probability distribution mainly corresponds to the Floquet-Gibbs state. This appears as the coupling  $\hat{\sigma}_{\pi/4}$  has a  $\sigma_z$  contribution so that the rates  $A_{\lambda\leftarrow\mu}^{(0)} \gg A_{\lambda\leftarrow\mu}^{(-1)}$  result mainly in a Gibbs state. However, the coefficients  $a_{\lambda\leftarrow\mu}^{(-1)}$  are almost equal to those of the  $\hat{\sigma}_{\pi/2}$  case and thus give rise to a probability jump, yet, to a very small extend.

Importantly, although there is a jump discontinuity, the density matrix remains continuous as a function of  $h_{z,1}$ . In the Floquet-Redfield formalism, the system density matrix reads  $\rho_s(t) = \sum_\lambda p_\lambda(t) |\varphi_\lambda(t)\rangle \langle \varphi_\lambda(t)|$ . As there is a simultaneous switch of  $p_\lambda$  and  $|\varphi_\lambda(t)\rangle$ , the

density matrix remains continuous. Yet, the probability jump does not depend on how the states  $\lambda = 0, 1$  are labeled, as the labeling can be uniquely defined. Let us consider the system with  $h_{z,0} \neq 0$ . A corresponding quasienergy spectrum is depicted in Fig. 2(a) with thin lines. For finite but small  $h_{z,0}$  the gap closing is released as depicted in Fig. 2(a). Accordingly, the states depend smoothly on  $h_{z,1}$ , so that the  $p_\lambda$  are also uniquely defined as can be observed in Fig. 2(b). The ordering of the states  $\lambda = 0, 1$  can be thus uniquely defined in terms of the limit  $h_{z,0} \rightarrow 0$ .

The interplay of  $\theta$  and  $h_{z,1}$  can be fully analyzed in Fig. 1(c), where the stationary state strongly depends on  $\theta$ , though, the system is only weakly coupled to the environment. In particular, for  $\theta \approx 0.5\pi$  and small  $h_{z,1}$  we find inversion,  $p_0 < 0.5$ , thus, there is a strong deviation from the Floquet-Gibbs state, which can be found for  $\theta = 0$ .

**Phonon emission.** Due to the continuous stationary state, the jump cannot be observed in system observables. However, the nonanalytic behavior can be observed in the emission. Every transition  $A_{\lambda\leftarrow\mu}^{(-1)}$  is related to the emission of phonons with either energy  $\Omega, \Omega \pm \Delta$ . The corresponding intensities  $I_{b,r} = I(\Omega \pm \Delta)$  are given by  $I_b = (\Omega + \epsilon_1 - \epsilon_0) A_{0\leftarrow 1}^{(-1)} p_1$ ,  $I_r = (\Omega - \epsilon_1 + \epsilon_0) A_{1\leftarrow 0}^{(-1)} p_0$ . We depict the blue and red shifted intensities in Fig. 3 (c) and (d). For  $\hat{\sigma}_{\pi/4}$ , we observe that the two intensities are almost equal. As the stationary state is governed by the rates  $A_{\lambda\leftarrow\mu}^{(-1)}$ , we find  $p_0 \propto A_{0\leftarrow 1}^{(-1)}$  and  $p_1 \propto A_{1\leftarrow 0}^{(-1)}$ , so that  $I_r \approx I_b$  for high frequency  $\Omega \gg \epsilon_1 - \epsilon_0$ .

For  $\hat{\sigma}_0 = \sigma_z$ , at which the system approaches a Floquet-Gibbs state, it is known that the rates  $A_{\mu\leftarrow\nu}^{n \neq 0} \approx 0$  [17]. Consequently, here both  $I_{r/b}$  vanish. Considering the difference  $I_b - I_r$  in Fig. 1(d), we consequently find that the difference is smooth in  $h_{z,1}$  for both limiting cases  $\theta = 0, \pi/2$ . However, in between there is a significant jump, which is strongest for about  $\theta \approx 0.3\pi$ .

Let us consider the  $\hat{\sigma}_{\pi/4}$  coupling. Due to the  $\sigma_z$  coupling component, the  $A_{\lambda\leftarrow\mu}^{(0)}$  rates are dominant, which leads to an (almost) thermalization of the system with its environment. However, the rates  $A_{\lambda\leftarrow\mu}^{(-1)}$  still exhibit a jump at the CDT, so that we find jumps in  $I_r$  and  $I_b$ , as can be observed in Fig. 3(d).

**Magnus expansion.** To find an appropriate approximation of the numerical results, we employ a rotating wave approximation defined by a unitary transformation [33]  $U_{\text{rot}}(t) = \exp[-i\sigma_z\theta(t)]$  with  $\theta(t) = \frac{h_{z,1}}{\Omega} \sin(\Omega t)$ . The resulting Hamiltonian  $H_r(t) = U_{\text{rot}}^\dagger \hat{H}(t) U_{\text{rot}}$  also exhibits  $\tau$  periodicity. The Floquet state propagator can be written as

$$e^{-i\hat{\Lambda}(t)} = \hat{U}_{\text{rot}}(t) e^{-i\hat{\Lambda}_r(t)} \approx \hat{U}_{\text{rot}}(t) [1 - i\hat{\Lambda}_r(t)] \quad (5)$$

with  $e^{-i\hat{\Lambda}_r(t)}$  being the Floquet state propagator in the rotating frame. The explicit form of  $\hat{\Lambda}_r$  can be calculated

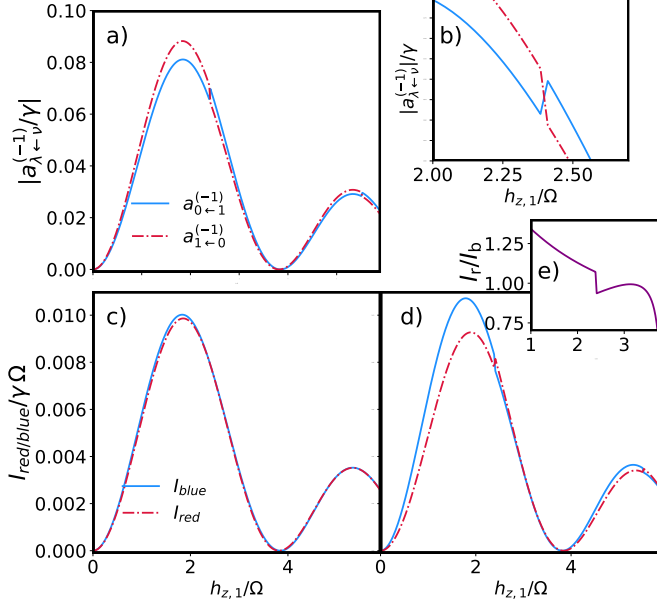


FIG. 3. (a) The transition coefficients for  $\hat{\sigma}_{\pi/2}$  with parameters equal to Fig. 1(c). The coefficients for  $\hat{\sigma}_{\pi/4}$  are almost equal. (b) Magnification of the jump discontinuity in (a). (c) and (d) depict corresponding intensities of blue and red shifted emitted phonons for  $\theta = \pi/2$  and  $\theta = \pi/4$  coupling, respectively. The ratio of the red and blue shifted emission is depicted in (e), their difference can be found in Fig. 1(d).

using a standard high frequency expansion [34]. However, using Eq. (5) without approximation, it is not possible to evaluate the integral in Eq. (3). As  $\hat{\Lambda}_r \propto \mathcal{O}(\frac{1}{\Omega})$  is small in the high frequency limit, the expansion in Eq. (5) is justified. For consistency, we also expand the Hamiltonian up to the same order, thus  $H_{\text{eff}} = H_{\text{eff}}^{(0)} + \frac{1}{\Omega} H_{\text{eff}}^{(1)} + \mathcal{O}(\frac{1}{\Omega^2})$ . Evaluating Eq. (3), we obtain

$$a_{\mu,\lambda}^{(n)} = \mathcal{S}_x^n \langle \sigma_x \rangle_{\mu\lambda} + i \cdot \mathcal{S}_y^n \langle \sigma_y \rangle_{\mu\lambda} + \mathcal{S}_z^n \langle \sigma_z \rangle_{\mu\lambda}, \quad (6)$$

where we have defined  $\langle \sigma_\alpha \rangle_{\mu\lambda} = \langle u_\mu(0) | \sigma_\alpha | u_\lambda(0) \rangle$  and

$$\begin{aligned} \mathcal{S}_x^n &= g_x \delta_{n \bmod 2, 0} \mathcal{J}_n \left( \frac{h_{z,1}}{\Omega} \right) - 2g_z \delta_{n,0} \sum_{k=1}^{\infty} l_{2k-1}, \\ &+ g_z \delta_{n \bmod 2, 1} l_{|n|}, \\ \mathcal{S}_y^n &= g_x \delta_{n \bmod 2, 1} \mathcal{J}_n \left( \frac{h_{z,1}}{\Omega} \right) - g_z \delta_{n \bmod 2, 0} l_{|n|}, \\ \mathcal{S}_z^n &= g_z \delta_{0,n} - g_z \mathcal{J}_{-n-2k} \left( \frac{h_{z,1}}{\Omega} \right) \delta_{n \bmod 2, 0} \sum_{k=1}^{\infty} l_{2k-1}, \\ &+ g_x \frac{1}{2} \delta_{n \bmod 2, 1} \alpha_x^{(n)}, \\ \alpha_x^{(n)} &= \sum_{m=1}^{\infty} l_m \left[ \mathcal{J}_{-n+m} \left( \frac{h_{z,1}}{\Omega} \right) - (-1)^m \mathcal{J}_{-n-m} \left( \frac{h_{z,1}}{\Omega} \right) \right], \end{aligned} \quad (7)$$

TABLE I. Coupling coefficients  $a_{\mu,\lambda}^{(n)}$  of all possible transitions between different Floquet states  $|\varphi_\lambda(0)\rangle$ .

$n=0$	$ -1\rangle_x$	$ +1\rangle_x$	$-1$	$ -1\rangle_x$	$ +1\rangle_x$
$ -1\rangle_x$	$\mathcal{S}_x^{(0)}$	$\mathcal{S}_z^{(0)}$	$ -1\rangle_x$	$\mathcal{S}_y^{(-1)}$	$\mathcal{S}_y^{(-1)} + \mathcal{S}_z^{(-1)}$
$ +1\rangle_x$	$\mathcal{S}_z^{(0)}$	$-\mathcal{S}_x^{(0)}$	$ +1\rangle_x$	$\mathcal{S}_y^{(-1)} - \mathcal{S}_z^{(-1)}$	$-\mathcal{S}_x^{(-1)}$

with  $g_x = \sin \theta$ ,  $g_z = \cos \theta$ ,  $l_m = \frac{h_x}{m\Omega} \mathcal{J}_m(h_z/\Omega)$  for  $m > 0$  and  $l_m = 0$  for  $m = 0$ . Due to the factor  $h_x/\Omega$  the coefficients  $l_n$  can be considered to be small.

The transition coefficients  $a_{\mu,\lambda}^{(n)}$  in Eq. (7) are evaluated in Tab. I. For  $n = 0$ , we find a hermitian structure for the eigenstates  $|\varphi_\lambda(0)\rangle \approx |-1\rangle_x, |+1\rangle_x$ , which are mainly determined by  $H_{\text{eff}}^{(0)} \propto \sigma_x$ . For  $n = -1$ , the transition coefficients are dominated by  $\mathcal{S}_y^{(-1)} \propto \mathcal{J}_{-1}(h_{z,1}/\Omega)$ , which explains the oscillations in Fig. 3(a). Importantly, they do not exhibit a hermitian structure. This leads to a breakdown of the detailed balance relation, and gives rise to the jump in the probability distribution in Fig. 2(b) and (c). This appears as  $|\varphi_0(0)\rangle$  switches from  $|-1\rangle_x$  to  $|+1\rangle_x$  and, simultaneously,  $|\varphi_1(0)\rangle$  switches from  $|+1\rangle_x$  to  $|-1\rangle_x$ , causing a jump of  $a_{\mu,\lambda}^{(-1)}$ .

We can use Eq. (6) to understand the intensity jump in the high-frequency regime. Assuming that  $p_\lambda \approx 0.5$  as in Fig. 2(b), we find for  $h_{z,1}/\Omega \approx z_0$

$$\frac{I_{\text{red}}}{I_{\text{blue}}} \approx \frac{\left( \mathcal{J}_{-1}(z_0) - \frac{h_x}{\Omega} \alpha_x^{(-1)}(z_0) \right)^2}{\left( \mathcal{J}_{-1}(z_0) + \frac{h_x}{\Omega} \alpha_x^{(-1)}(z_0) \right)^2} \approx 1 \pm 2 \frac{h_x}{\Omega} \alpha_x^{(-1)}(z_0)$$

with a constant  $\alpha_x^{(-1)}(z_0)$ , and '±' for  $h_z/\Omega \lessgtr z_0$ . Thus, interestingly, this ratio (Fig. 3(e)) close to the CDT and consequently the jump magnitude  $4 \frac{h_x}{\Omega} \alpha_x^{(-1)}(z_0)$  scales as  $1/\Omega$ .

**Discussion.** The CDT in a driven dissipative system gives rise to surprising effects. Besides the well-investigated freezing of the internal system dynamics at the CDT, the presence of the thermal environment can give rise to counter intuitive jumps in the probability distribution of the Floquet state. Yet, as there is a simultaneous switch of Floquet states and probability, the reduced density matrix remains continuous while crossing the CDT. Consequently, the probability jumps can not be observed in system observables. Moreover, the jump behavior has a drastic consequence on the Mollow triplet, such that the blue and red shifted intensities both exhibit a discontinuity at the CDT. This can be directly measured by phonon spectroscopy. The ratio of both shifted intensities exhibits a jump of about 10%.

The underlying physical reason for these discontinuities is a switch of the Floquet states at the CDT. This causes a jump in the system-bath coupling coefficients. Consequently, the effect does not depend on the details of the thermal bath. Yet, the system-bath coupling operator is important. For a pure  $\hat{\sigma}_0 = \sigma_z$  coupling as inves-

tigated in Ref. [17], the stationary density matrix of the system recovers an effective Floquet-Gibbs states. For  $\hat{\sigma}_{\pi/2} = \sigma_x$ , we find extreme deviations from the Floquet-Gibbs state with occupation inversion even for small driving amplitude as observed in Fig. 2(b). With this coupling, the probability jump at the CDT turns out to be most significant. However, there is no signature in the emitted phonons. For  $\hat{\sigma}_{\pi/4}$  coupling, though the probability jumps are very small, there is a clear jump discontinuity in the blue and red shifted intensity.

The noncontinuous behaviour is not a consequence of the high-frequency regime, which we considered here to explain the numerical results with analytical calculations. The CDT appears due to an exact degeneracy of the quasienergies which is persistent even for very low driving-frequencies [30]. Consequently, the jump behavior will remain when lowering the driving frequency. Our findings are not restricted to the dissipative two-level system. Similar probability jumps could be also observed in dissipative driven Lipkin-Meshkov-Glick model, which

gives rise to many-body CDT [33]. Furthermore, these findings will be important for electronic transport [35–37]. It will be interesting to explore the fate of the jumps for stronger environmental coupling using methods such as [38–42]

Finally, the analytical treatment based on the Magnus expansion extended with our approximation Eq. (5) is the key tool to understand the discontinuities. The analytical treatment can be generalized to other configurations of the driving which could give rise to even more flexible mechanisms of the stationary state, and other exotic stationary states in driven systems.

**Acknowledgments.** G. Engelhardt gratefully acknowledges financial support from the China Postdoc Science Foundation (Grant No.: 2018M640054), J. Cao acknowledges support from the NSF (Grant No.: CHE 1800301 and CHE 1836913). Both acknowledge the Natural Science Foundation of China (under Grant No.: U1530401). G. Platero acknowledges MINECO (Grant No.: MAT2017-86717-P). The authors thank Hui Dong and Tilen Čadež for inspiring discussions

- 
- [1] M. Aidelsburger, M. Atala, M. Lohse, J. T. Barreiro, B. Paredes, and I. Bloch, “Realization of the Hofstadter Hamiltonian with ultracold atoms in optical lattices,” *Phys. Rev. Lett.* **111**, 185301 (2013).
  - [2] G. Jotzu, M. Messer, R. Desbuquois, M. Lebrat, T. Uehlinger, D. Greif, and T. Esslinger, “Experimental realization of the topological Haldane model with ultracold fermions,” *Nature (London)* **515**, 237–240 (2014).
  - [3] M. Benito, A. Gómez-León, V. M. Bastidas, T. Brandes, and G. Platero, “Floquet engineering of long-range  $p$ -wave superconductivity,” *Phys. Rev. B* **90**, 205127 (2014).
  - [4] G. Engelhardt, M. Benito, G. Platero, and T. Brandes, “Topologically enforced bifurcations in superconducting circuits,” *Phys. Rev. Lett.* **118**, 197702 (2017).
  - [5] V. M. Bastidas, C. Emary, B. Regler, and T. Brandes, “Nonequilibrium quantum phase transitions in the Dicke model,” *Phys. Rev. Lett.* **108**, 043003 (2012).
  - [6] G. Engelhardt, M. Benito, G. Platero, and T. Brandes, “Topological instabilities in ac-driven bosonic systems,” *Phys. Rev. Lett.* **117**, 045302 (2016).
  - [7] G. Engelhardt, V. M. Bastidas, C. Emary, and T. Brandes, “ac-driven quantum phase transition in the Lipkin-Meshkov-Glick model,” *Phys. Rev. E* **87**, 052110 (2013).
  - [8] J. Liu, C.-Y. Hsieh, and J. Cao, “Efficiency at maximum power of a quantum carnot engine with temperature tunable baths,” *arXiv:1710.06565* (2017).
  - [9] G. Platero and R. Aguado, “Photon-assisted transport in semiconductor nanostructures,” *Physics Reports* **395**, 1–157 (2004).
  - [10] R. Bavli and H. Metiu, “Properties of an electron in a quantum double well driven by a strong laser: Localization, low-frequency, and even-harmonic generation,” *Phys. Rev. A* **47**, 3299–3310 (1993).
  - [11] Y. Dakhnovskii and R. Bavli, “Emission spectrum and localization of electrons in quantum-well systems induced by a strong laser field,” *Phys. Rev. B* **48**, 11020–11023 (1993).
  - [12] P.R. Graves and D. Gardiner, *Practical Raman spectroscopy* (Springer, 1989).
  - [13] N. Mann, M. Reza Bakhtiari, F. Massel, A. Pelster, and M. Thorwart, “Driven bose-hubbard model with a parametrically modulated harmonic trap,” *Phys. Rev. A* **95**, 043604 (2017).
  - [14] A. Komnik and M. Thorwart, “BCS theory of driven superconductivity,” *Eur. Phys. J. B* **89**, 244 (2016).
  - [15] F. Grossmann, T. Dittrich, P. Jung, and P. Hänggi, “Coherent destruction of tunneling,” *Phys. Rev. Lett.* **67**, 516–519 (1991).
  - [16] B. R. Mollow, “Power spectrum of light scattered by two-level systems,” *Phys. Rev.* **188**, 1969–1975 (1969).
  - [17] T. Shirai, T. Mori, and S. Miyashita, “Condition for emergence of the Floquet-Gibbs state in periodically driven open systems,” *Phys. Rev. E* **91**, 030101 (2015).
  - [18] T. Shirai, J. Thingna, T. Mori, S. Denisov, P. Hänggi, and S. Miyashita, “Effective Floquet-Gibbs states for dissipative quantum systems,” *New Journal of Physics* **18**, 053008 (2016).
  - [19] M. Frasca, “Perturbative results on localization for a driven two-level system,” *Phys. Rev. B* **68**, 165315 (2003).
  - [20] J. T. Stockburger, “Stabilizing coherent destruction of tunneling,” *Phys. Rev. E* **59**, R4709–R4712 (1999).
  - [21] J. C. A. Barata and W. F. Wreszinski, “Strong-coupling theory of two-level atoms in periodic fields,” *Phys. Rev. Lett.* **84**, 2112–2115 (2000).
  - [22] B. Pigeau, S. Rohr, L. M. De Lepinay, A. Gloppe, V. Jacques, and O. Arcizet, “Observation of a phononic Mollow triplet in a multimode hybrid spin-nanomechanical system,” *Nature Communications* **6**, 8603–8603 (2015).
  - [23] Y. Yan, Z. Lu, and H. Zheng, “Resonance fluorescence of strongly driven two-level system coupled to multiple dissipative reservoirs,” *Annals of Physics* **371**, 159–182 (2015).

- (2016).
- [24] C. Duan, C.-Y. Hsieh, Liu J., and J. Cao, “Unusual transport properties with non-commutative system-bath coupling operators,” In preparation.
  - [25] A. H. Castro Neto, E. Novais, L. Borda, Gergely Zaránd, and I. Affleck, “Quantum magnetic impurities in magnetically ordered systems,” *Phys. Rev. Lett.* **91**, 096401 (2003).
  - [26] Cheng Guo, Andreas Weichselbaum, Jan von Delft, and Matthias Vojta, “Critical and strong-coupling phases in one- and two-bath spin-boson models,” *Phys. Rev. Lett.* **108**, 160401 (2012).
  - [27] Heiner Kohler, Andreas Hackl, and Stefan Kehrein, “Nonequilibrium dynamics of a system with quantum frustration,” *Phys. Rev. B* **88**, 205122 (2013).
  - [28] Benedikt Bruognolo, Andreas Weichselbaum, Cheng Guo, Jan von Delft, Imke Schneider, and Matthias Vojta, “Two-bath spin-boson model: Phase diagram and critical properties,” *Phys. Rev. B* **90**, 245130 (2014).
  - [29] J. H. Shirley, “Solution of the Schrödinger equation with a Hamiltonian periodic in time,” *Phys. Rev.* **138**, B979–B987 (1965).
  - [30] M. Grifoni and P. Hänggi, “Driven quantum tunneling,” *Physics Reports* **304**, 229–354 (1998).
  - [31] J. C. L. Carreno, E. D. Valle, and F. P. Laussy, “Photon correlations from the Mollow triplet,” *Laser & Photonics Reviews* **11**, 1700090 (2017).
  - [32] Due to  $\sigma_z H_s(t) \sigma_z = H_s(t + \tau/2)$ , the Floquet states fulfill  $\sigma_z |\phi_\lambda(t)\rangle = u_\lambda |\phi_{\lambda+\tau/2}(t)\rangle$  with  $u_\lambda \in \{-1, 1\}$  and  $u_0 \neq u_1$ . Using this in Eq. (3) shows that  $A_{\lambda \leftarrow \mu}^{(0)} = 0$  for  $\lambda \neq \mu$ .
  - [33] J. Gong, L. Moralesmolina, and P. Hänggi, “Many-body coherent destruction of tunneling,” *Phys. Rev. Lett.* **103**, 133002 (2009).
  - [34] E. S. Mananga and T. Charpentier, “Introduction of the Floquet-Magnus expansion in solid-state nuclear magnetic resonance spectroscopy,” *Journal of Chemical Physics* **135**, 044109 (2011).
  - [35] R. Sánchez, G. Platero, and T. Brandes, “Resonance fluorescence in driven quantum dots: Electron and photon correlations,” *Phys. Rev. B* **78**, 125308 (2008).
  - [36] T. Brandes, R. Aguado, and G. Platero, “Charge transport through open driven two-level systems with dissipation,” *Phys. Rev. B* **69**, 205326 (2004).
  - [37] R. Sánchez, G. Platero, and T. Brandes, “Resonance fluorescence in transport through quantum dots: Noise properties,” *Phys. Rev. Lett.* **98**, 146805 (2007).
  - [38] S. Restrepo, J. Cerrillo, V. M. Bastidas, D. G. Angelakis, and T. Brandes, “Driven open quantum systems and Floquet stroboscopic dynamics,” *Phys. Rev. Lett.* **117**, 250401 (2016).
  - [39] L. Magazzù, S. Denisov, and P. Hänggi, “Asymptotic Floquet states of a periodically driven spin-boson system in the nonperturbative coupling regime,” *Phys. Rev. E* **98**, 022111 (2018).
  - [40] D. Xu and J. Cao, “Non-canonical distribution and non-equilibrium transport beyond weak system-bath coupling regime: A polaron transformation approach,” *Frontiers of Physics* **11**, 110308 (2016).
  - [41] C. Duan, Z. Tang, J. Cao, and J. Wu, “Zero-temperature localization in a sub-ohmic spin-boson model investigated by an extended hierarchy equation of motion,” *Phys. Rev. B* **95**, 214308 (2017).
  - [42] C. K. Lee, J. Cao, and J. Gong, “Noncanonical statistics of a spin-boson model: Theory and exact monte carlo simulations,” *Phys. Rev. E* **86**, 021109 (2012).

## Supplementary information

In this supplementary information we explicitly show how to derive the analytical expression for the Floquet states transition elements Eq. (3) in the high-frequency regime, which is given in Eq. (6). According to Floquet theory, the time-evolution operator can be written as

$$\hat{U}(t, 0) = e^{-i\hat{\Lambda}(t)} e^{-iH_{\text{eff}}(t)} \quad (8)$$

with a time-periodic hermitian operator  $\hat{\Lambda}(t)$  and a Floquet Hamiltonian  $H_{\text{eff}}$  whose eigenvalues and eigenstates represent quasienergies and stroboscopic Floquet states respectively.

### I. TRANSFORMATION INTO A ROTATING FRAME

The system Hamiltonian describing the isolated spin system reads

$$H_s = \frac{h_x}{2} \sigma_x + \frac{h_{z,1}}{2} \cos(\Omega t) \sigma_z, \quad (9)$$

where we consider the case  $h_{z,0} = 0$  for simplicity. The transformation into a rotating frame is defined by the unitary operator

$$\begin{aligned} \hat{U}_{\text{rot}}(t) &= \exp[-i\sigma_z \theta(t)], \\ \theta(t) &= \frac{h_{z,1}}{2\Omega} \sin(\Omega t), \end{aligned} \quad (10)$$

which transforms the system wave function  $|\Psi(t)\rangle = \hat{U}_{\text{rot}}^\dagger(t) |\tilde{\Psi}(t)\rangle$ , with  $|\tilde{\Psi}(t)\rangle$  being the wave function in the rotating frame.

Evaluating the expressions of the unitary operators, we find

$$U_{\text{rot}}(t) = 1 \cdot \cos \theta(t) - i\sigma_z \sin \theta(t), \quad (11)$$

which gives rise to the transformation of the Pauli operators

$$\begin{aligned} U_{\text{rot}}^\dagger(t) \sigma_z U_{\text{rot}}(t) &= \sigma_z, \\ U_{\text{rot}}^\dagger(t) \sigma_x U_{\text{rot}}(t) &= [\cos^2(\theta) - \sin^2(\theta)] \sigma_x + \cos(\theta) \sin(\theta) i [\sigma_z \sigma_x - \sigma_x \sigma_z], \\ &= \cos(2\theta) \sigma_x - \sin(2\theta) \sigma_y, \\ U_{\text{rot}}^\dagger(t) \sigma_y U_{\text{rot}}(t) &= \cos(2\theta) \sigma_y + \sin(2\theta) \sigma_x. \end{aligned} \quad (12)$$

## II. ROTATING WAVE APPROXIMATION

This can be expanded as a Fourier decomposition

$$H_s(t) = \sum_{n=-\infty}^{\infty} H_s^{(n)} e^{in\Omega t}, \quad (13)$$

at which each Fourier component reads

$$H_s^{(n)} = \frac{h_x}{2} \mathcal{J}_n \left( \frac{h_{z,1}}{\Omega} \right) \begin{cases} \sigma_x & n \text{ even} \\ i\sigma_y & n \text{ odd} \end{cases}, \quad (14)$$

where we have used the integral representation of the Bessel functions

$$J_n(x) = \frac{1}{2\pi} \int_{-\pi}^{\pi} e^{x \sin \tau + n\tau} d\tau \quad (15)$$

Following Ref. [34], a high-frequency expansion of the system time-evolution operator in Eq. (8) reads

$$\begin{aligned} H_{\text{eff}} &= H_s^{(0)} + \frac{1}{2} \sum_{m \neq 0} \frac{1}{m\omega} [H_s^{(m)}, H_s^{(-m)}] + \sum_{m \neq 0} \frac{1}{m\omega} [H_s^{(0)}, H_s^{(-m)}] + \mathcal{O}\left(\frac{1}{\Omega}\right), \\ \hat{\Lambda}(t) &= \sum_{n \neq 0} \frac{1}{in\Omega} H_s^{(n)} (e^{in\Omega t} - 1) + \mathcal{O}\left(\frac{1}{\Omega^2}\right) \end{aligned} \quad (16)$$

where we consider the lowest non-vanishing terms in order of  $\frac{1}{\Omega}$ . For the system under consideration, we find the well-known result

$$H_{\text{eff}} = \frac{h_x}{2} \mathcal{J}_0(h_{z,1}/\Omega) \sigma_x - 2 \frac{h_x^2}{\Omega} \sum_{k>0} \frac{\mathcal{J}_{2k-1}(h_{z,1}/\Omega)}{2k-1} \sigma_z + \mathcal{O}\left(\frac{1}{\Omega}\right) \quad (17)$$

and

$$\begin{aligned} \hat{\Lambda}(t) &= \frac{h_x}{2} \sum_{k=1}^{\infty} \frac{1}{2k\Omega} \mathcal{J}_{2k} \left( \frac{h_{z,1}}{\Omega} \right) 2 \sin(2k\Omega t) \sigma_x + \frac{h_x}{2} \sum_{k=1}^{\infty} \frac{1}{(2k-1)\Omega} \mathcal{J}_{(2k-1)} \left( \frac{h_{z,1}}{\Omega} \right) 2(\cos((2k-1)\Omega t) - 1) \sigma_y + \mathcal{O}\left(\frac{1}{\Omega^2}\right) \\ &= \frac{h_x}{\Omega} \sum_{k=1}^{\infty} l_{2k} \sin(2k\Omega t) \sigma_x + \frac{h_x}{\Omega} \sum_{k=1}^{\infty} l_{2k-1} (\cos((2k-1)\Omega t) - 1) \sigma_y + \mathcal{O}\left(\frac{1}{\Omega^2}\right) \\ &= \frac{h_x}{\Omega} l_x(t) \sigma_x + \frac{h_x}{\Omega} l_y(t) \sigma_y + \mathcal{O}\left(\frac{1}{\Omega^2}\right), \end{aligned} \quad (18)$$

where  $l_n(z) = \frac{1}{n\Omega} \mathcal{J}_n(z)$ . We use this to calculate the terms  $a_{\mu,\lambda}^{(n)}$

$$\begin{aligned} a_{\mu,\lambda}^{(n)} &= \frac{1}{\tau} \int_0^\tau \langle u_\mu(t) | \hat{\sigma}_\theta | u_\lambda(t) \rangle e^{-in\Omega t} dt \\ &= \frac{1}{\tau} \int_0^\tau \langle u_\mu(0) | e^{i\hat{\Lambda}(t)} U_{\text{rot}}^\dagger [g_x \sigma_x + g_z \sigma_z] U_{\text{rot}} e^{-i\hat{\Lambda}(t)} | u_\lambda(0) \rangle e^{-in\Omega t} dt \end{aligned} \quad (19)$$

Using the expansion

$$e^{-i\hat{\Lambda}(t)} \approx 1 - i\hat{\Lambda}(t), \quad (20)$$

we can explicitly solve the integral and find

$$a_{\mu,\lambda}^{(n)} = g_x a_{x,\mu,\lambda}^{(n)} + g_z a_{z,\mu,\lambda}^{(n)}, \quad (21)$$

with

$$\begin{aligned} a_{x,\mu,\lambda}^{(n)} &= \frac{1}{\tau} \int_0^\tau \langle u_\mu(0) | e^{i\hat{\Lambda}(t)} [\cos(2\theta) \sigma_x - \sin(2\theta) \sigma_y] e^{-i\hat{\Lambda}(t)} | u_\lambda(0) \rangle e^{-in\Omega t} dt \\ &\approx \frac{h_x}{\Omega} \frac{1}{\tau} \int_0^\tau \langle u_\mu(0) | \left[ \cos(2\theta) \left[ \sigma_x + i \frac{h_x}{\Omega} l_y(t) [\sigma_y, \sigma_x] \right] - \sin(2\theta) \left[ \sigma_y + i \frac{h_x}{\Omega} l_x(t) [\sigma_x, \sigma_y] \right] \right] | u_\lambda(0) \rangle e^{-in\Omega t} dt \\ &= \frac{h_x}{\Omega} \frac{1}{\tau} \int_0^\tau \langle u_\mu(0) | \cos(2\theta) \sigma_x - \sin(2\theta) \sigma_y + 2 \frac{h_x}{\Omega} [l_y(t) \cos(2\theta) + l_x(t) \sin(2\theta)] \sigma_z | u_\lambda(0) \rangle e^{-in\Omega t} dt, \\ a_{z,\mu,\lambda}^{(n)} &= \frac{h_x}{\Omega} \frac{1}{\tau} \int_0^\tau \langle u_\mu(0) | e^{i\hat{\Lambda}(t)} \sigma_z e^{-i\hat{\Lambda}(t)} | u_\lambda(0) \rangle e^{-in\Omega t} dt \\ &\approx \frac{h_x}{\Omega} \frac{1}{\tau} \int_0^\tau \langle u_\mu(0) | \sigma_z + i \frac{h_x}{\Omega} l_y(t) [\sigma_y, \sigma_z] + i \frac{h_x}{\Omega} l_x(t) [\sigma_x, \sigma_z] | u_\lambda(0) \rangle e^{-in\Omega t} dt \\ &= \frac{h_x}{\Omega} \frac{1}{\tau} \int_0^\tau \langle u_\mu(0) | \sigma_z - 2 \frac{h_x}{\Omega} l_y(t) \sigma_x + 2 \frac{h_x}{\Omega} l_x(t) \sigma_y | u_\lambda(0) \rangle e^{-in\Omega t} dt \end{aligned} \quad (22)$$

This integrals can be solved analytically, giving

$$\begin{aligned} a_{x,\mu,\lambda}^{(n)} &= \frac{1}{2} \left[ \mathcal{J}_{-n} \left( \frac{h_{z,1}}{\Omega} \right) + \mathcal{J}_{-n} \left( -\frac{h_{z,1}}{\Omega} \right) \right] \langle u_\mu(0) | \sigma_x | u_\lambda(0) \rangle \\ &\quad - \frac{1}{2i} \left[ \mathcal{J}_{-n} \left( \frac{h_{z,1}}{\Omega} \right) - \mathcal{J}_{-n} \left( -\frac{h_{z,1}}{\Omega} \right) \right] \langle u_\mu(0) | \sigma_y | u_\lambda(0) \rangle \\ &\quad + \frac{h_x}{\Omega} \mathcal{A}_x^{(n)} \langle u_\mu(0) | \sigma_z | u_\lambda(0) \rangle \\ &= \mathcal{J}_n \left( \frac{h_{z,1}}{\Omega} \right) \delta_{n \bmod 2, 0} \langle \sigma_x \rangle_{\mu\lambda} - i \mathcal{J}_n \left( \frac{h_{z,1}}{\Omega} \right) \delta_{n \bmod 2, 1} \langle \sigma_y \rangle_{\mu\lambda} + \mathcal{A}_x^{(n)} \langle \sigma_z \rangle_{\mu\lambda}, \end{aligned} \quad (23)$$

and

$$a_{z,\mu,\lambda}^{(n)} = \mathcal{B}_x^{(n)} \langle \sigma_x \rangle_{\mu\lambda} + \mathcal{B}_y^{(n)} \langle \sigma_y \rangle_{\mu\lambda} + \delta_{n,0} \langle \sigma_z \rangle_{\mu\lambda}, \quad (24)$$

where we have defined

$$\mathcal{A}_x^{(n)} = \frac{1}{\tau} \int_0^\tau 2 [l_y(t) \cos(2\theta) + l_x(t) \sin(2\theta)] e^{-in\Omega t} dt = \mathcal{A}_{x,1}^{(n)} + \mathcal{A}_{x,2}^{(n)} \quad (25)$$

Evaluating these terms we obtain

$$\mathcal{A}_{x,1}^{(n)} = \frac{1}{\tau} \int_0^\tau 2 \frac{h_x}{\Omega} l_y(t) \cos(2\theta) e^{-in\Omega t} dt = 2 \sum_{k=1}^{\infty} \frac{h_x}{\Omega} l_{2k-1} \frac{1}{\tau} \int_0^\tau \cos(2\theta) (\cos((2k-1)\Omega t) - 1) e^{-in\Omega t} dt$$



$$\begin{aligned}
&= \sum_{k=1}^{\infty} \frac{h_x}{\Omega} l_{2k-1} \left[ -\mathcal{J}_{-n} \left( \frac{h_{z,1}}{\Omega} \right) - \mathcal{J}_{-n} \left( -\frac{h_{z,1}}{\Omega} \right) \right. \\
&\quad + \frac{1}{2} \mathcal{J}_{-n+2k-1} \left( \frac{h_{z,1}}{\Omega} \right) + \frac{1}{2} \mathcal{J}_{-n+2k-1} \left( -\frac{h_{z,1}}{\Omega} \right) \\
&\quad \left. + \frac{1}{2} \mathcal{J}_{-n-2k+1} \left( \frac{h_{z,1}}{\Omega} \right) + \frac{1}{2} \mathcal{J}_{-n-2k+1} \left( -\frac{h_{z,1}}{\Omega} \right) \right] \\
&= \sum_{k=1}^{\infty} \frac{h_x}{\Omega} l_{2k-1} \left[ -\mathcal{J}_{-n} \left( \frac{h_{z,1}}{\Omega} \right) (1 + (-1)^n) \right. \\
&\quad + \frac{1}{2} \mathcal{J}_{-n+2k-1} \left( \frac{h_{z,1}}{\Omega} \right) (1 + (-1)^{-n+2k-1}) \\
&\quad \left. + \frac{1}{2} \mathcal{J}_{-n-2k+1} \left( \frac{h_{z,1}}{\Omega} \right) (1 + (-1)^{-n-2k+1}) \right] \\
&= \sum_{k=1}^{\infty} \frac{h_x}{\Omega} l_{2k-1} \left[ -\mathcal{J}_{-n} \left( \frac{h_{z,1}}{\Omega} \right) (1 + (-1)^n) \right. \\
&\quad + \frac{1}{2} \mathcal{J}_{-n+2k-1} \left( \frac{h_{z,1}}{\Omega} \right) (1 - (-1)^{-n}) \\
&\quad \left. - (-1)^{(2k-1)} \frac{1}{2} \mathcal{J}_{-n-2k+1} \left( \frac{h_{z,1}}{\Omega} \right) (1 - (-1)^{-n}) \right] \tag{26}
\end{aligned}$$

$$\begin{aligned}
\mathcal{A}_{x,2}^{(n)} &= \frac{1}{\tau} \int_0^{\tau} 2 \frac{h_x}{\Omega} l_y(t) \sin(2\theta) e^{-in\Omega t} dt = 2 \sum_{k=1}^{\infty} l_{2k-1} \frac{1}{\tau} \int_0^{\tau} \sin(2\theta) \sin(2k\Omega t) e^{-in\Omega t} dt \\
&= - \sum_{k=1}^{\infty} l_{2k} \left[ + \frac{1}{2} \mathcal{J}_{-n+2k} \left( \frac{h_{z,1}}{\Omega} \right) - \frac{1}{2} \mathcal{J}_{-n+2k} \left( -\frac{h_{z,1}}{\Omega} \right) \right. \\
&\quad \left. - \frac{1}{2} \mathcal{J}_{-n-2k} \left( \frac{h_{z,1}}{\Omega} \right) + \frac{1}{2} \mathcal{J}_{-n-2k} \left( -\frac{h_{z,1}}{\Omega} \right) \right] \\
&= - \sum_{k=1}^{\infty} l_{2k} \left[ + \frac{1}{2} \mathcal{J}_{-n+2k} \left( \frac{h_{z,1}}{\Omega} \right) (1 - (-1)^{-n+2k}) \right. \\
&\quad \left. - \frac{1}{2} \mathcal{J}_{-n-2k} \left( \frac{h_{z,1}}{\Omega} \right) (1 - (-1)^{-n-2k}) \right] \\
&= - \sum_{k=1}^{\infty} l_{2k} \left[ + \frac{1}{2} \mathcal{J}_{-n+2k} \left( \frac{h_{z,1}}{\Omega} \right) (1 - (-1)^{-n}) - (-1)^{2k} \frac{1}{2} \mathcal{J}_{-n-2k} \left( \frac{h_{z,1}}{\Omega} \right) (1 - (-1)^{-n}) \right] \tag{27}
\end{aligned}$$

$$\begin{aligned}
\mathcal{A}_1^{(n)} &= -\mathcal{J}_n \left( \frac{h_{z,1}}{\Omega} \right) \delta_{n \bmod 2,0} \sum_{k=1}^{\infty} l_{2k-1} \\
&\quad + \frac{1}{2} \delta_{n \bmod 2,1} \sum_{m=1}^{\infty} l_m \left[ \mathcal{J}_{-n+m} \left( \frac{h_{z,1}}{\Omega} \right) - (-1)^m \mathcal{J}_{-n-m} \left( \frac{h_{z,1}}{\Omega} \right) \right] \tag{28}
\end{aligned}$$

$$\begin{aligned}
\mathcal{B}_{x,1}^{(n)} &= \frac{1}{\tau} \int_0^{\tau} 2 l_y(t) e^{-in\Omega t} dt = 2 \sum_{k=1}^{\infty} l_{2k-1} \frac{1}{\tau} \int_0^{\tau} (\cos((2k-1)\Omega t) - 1) e^{-in\Omega t} dt \\
&= \sum_{k=1}^{\infty} l_{2k-1} [-2\delta_{n,0} + \delta_{2k-1-n,0} + \delta_{-2k-1-n,0}] = -2\delta_{n,0} \sum_{k=1}^{\infty} l_{2k-1} + \delta_{n \bmod 2,1} l_{|n|} \tag{29}
\end{aligned}$$

$$\begin{aligned}
\mathcal{B}_{y,1}^{(n)} &= \frac{1}{\tau} \int_0^\tau 2l_x(t) e^{-in\Omega t} dt = 2 \sum_{k=1}^{\infty} l_{2k} \frac{1}{\tau} \int_0^\tau \sin(k\Omega t) e^{-in\Omega t} dt \\
&= \frac{1}{i} \sum_{k=1}^{\infty} l_{2k} [\delta_{2k-n,0} - \delta_{-2k-n,0}] = -i \delta_{n \bmod 2, 0} l_{|n|}
\end{aligned} \tag{30}$$


---